Journal of Biomedical Materials Research Part B: Applied Biomaterials

WILEY

Society For Biomaterials

RESEARCH ARTICLE

Taguchi Optimization of Additively Manufactured PEKK and Silicon Nitride Loaded PEKK for Medical Device Applications

Tabitha Derr[1] | Cemile Basgul[1] | Paul DeSantis[1] | Ryan M. Bock[2] | Steven M. Kurtz[1]

[1]Implant Research Core, Drexel University, Philadelphia, Pennsylvania, USA | [2]Sintx Technologies, Inc, Salt Lake City, Utah, USA

Correspondence: Tabitha Derr (td627@drexel.edu)

Received: 28 July 2025 | **Revised:** 20 November 2025 | **Accepted:** 24 November 2025

Keywords: additive manufacturing | fused filament fabrication | polyetherketoneketone | silicon nitride | Taguchi

ABSTRACT

Silicon nitride (Si_3N_4) is reported to exhibit antibacterial properties and support osteoblast maturation, while polyetherketoneketone (PEKK) is considered to potentially have antibacterial and osseointegrative properties while offering favorable manufacturability through extrusion-based additive manufacturing compared to traditional ceramics manufacturing. Incorporating silicon nitride into PEKK is hypothesized to enhance its bioactivity while maintaining processability, making Si_3N_4-PEKK composites promising for medical implants. Our objective was to determine optimal fused filament fabrication (FFF) parameters for PEKK and Si_3N_4-PEKK. Taguchi optimization (L9 array, $n = 5$) was performed on PEKK and 15 vol.% Si_3N_4-PEKK to assess the impact of printing parameters (layer height: 0.1, 0.2, and 0.3 mm; nozzle temperature (PEKK/Si_3N_4-PEKK): 340/380, 370/400, and 400/420; bed temperature: 130°C, 150°C, and 170°C; and chamber temperature: 110°C, 130°C, and 150°C) on ultimate tensile strength (UTS). Z-directional tensile specimens were printed on a medical FFF printer. Specimens underwent tensile testing according to ASTM D638. Signal/noise ratios for UTS were calculated and ANOVA (Minitab 21.4.2) was used to assess statistical significance ($p < 0.05$). Layer height had the greatest impact on UTS for both PEKK and Si_3N_4-PEKK. Optimal nozzle and chamber temperatures were 400°C and 130°C, respectively, while the optimal layer height was 0.1 mm for both materials. The optimal bed temperature for PEKK and Si_3N_4-PEKK was 150°C and 170°C, respectively. For PEKK, differences in all parameters were significant except for bed temperature, while for Si_3N_4-PEKK all parameters were significant except for nozzle temperature. The specimens with optimum statistically significant parameters showed the highest UTS for both PEKK (91 ± 2 MPa) and Si_3N_4-PEKK (76 ± 3 MPa). Layer height is the most influential printing variable for both PEKK and Si_3N_4-PEKK. The optimal PEKK printing condition has a comparable UTS, while Si_3N_4-PEKK achieved 84% of the injection-molded value for neat PEKK.

1 | Introduction

Infection and bone integration remain critical issues across orthopedic, craniomaxillofacial, and spinal implants [1]. In addition to the potential health risks, infections can create a significant economic burden [2], driving research into various strategies to reduce infection, from modifying surgical conditions to reduce infection risk through passive and active surface modifications for antibacterial implant surfaces [3]. Of particular interest are potential biomaterials that have inherent anti-infective properties. Silicon nitride (Si_3N_4) is a ceramic with reported antibacterial and osseointegrative properties. Its antibacterial effects have been attributed to surface topography, negative surface charge, and ammonia elution [4–8]. Additionally, its hydrophilicity, induced by polar surface moieties, has been suggested to enhance protein adsorption and promote bone formation [9–11]. Although Si_3N_4 can be used to fabricate all-ceramic implants, its high elastic modulus may lead to stress

shielding, subsidence, and increased risk of brittle fracture [12]. Additionally, the manufacturability of this ceramic via additive manufacturing techniques, like digital light processing (DLP) or stereolithography (SLA), is quite difficult due to absorption of UV or laser energy and difficulty curing, while more traditional ceramic manufacturing is time intensive with sintering and machining. Therefore, using Si_3N_4 in a composite with a PAEK polymer may combine Si_3N_4's bioactive properties with a modulation of its mechanical properties and allow for additive manufacturing techniques.

With the advent of 3D printing, polyaryletherketones (PAEKs) have gained further interest in medical applications, due to their mechanical properties, which more closely align with bone compared to metallic implants [13], as well as their ability to be fabricated using fused filament technology to create complex geometries and incorporate porosity [14]. Historically, polyetheretherketone (PEEK) is most commonly used in spinal fusion and cranioplasty [15–18], however, 3D printing of PEEK remains challenging due to its high processing temperature [15], and it lacks antibacterial or osseointegrative properties, as it is hydrophobic and largely inert [19]. An alternative emerging PAEK in the medical field is polyetherketoneketone (PEKK), which exists in several standard grades due to the ratio of the terephthalic and isophthalic isomers (T/I). Modulation of this ratio allows for control of the crystallization behavior, with lower ratios, such as the 60/40 T/I that is commonly used in PEKK printing filaments, having mechanical properties similar to PEEK but with lower processing temperatures [20], making it easier to 3D print via FFF. Additionally, surface modified PEKK has been proposed to have some antibacterial properties [21] while chemically surface modified PEKK also showed enhanced osseointegrative properties [22] compared to similarly modified PEEK; however, it is important to note that both studies included surface modification and do not speak to unmodified PEKK.

While FFF printing of PEEK has been well studied, the impact of printing parameters on the mechanical properties of PEKK remains less understood [23–27]. While a few studies have focused on optimizing printing parameters for the flexural properties of PEKK [28–30], fewer have looked at optimizing tensile strength [31, 32]. Although, these studies investigated the tensile strength of FFF PEKK, Rashed et al. [32] did not examine any thermal printing parameters and Magri et al. [31] did not use any experimental design methods to robustly test multiple print parameters. In addition, neither investigated the effect of printing parameters on vertically printed tensile specimens. An additional study on 3D printed PEKK analyzed the effect of print orientation; however, they did not optimize any of the printing parameters [33]. Doyle et al. [33] found a reduction in strength in the *z*-direction for PEKK, supporting the conclusion that this orientation exhibits the weakest adhesion strength of the print directions and requires additional optimization. Furthermore, the effect of the silicon nitride particles on the mechanical properties of 3D printed PEKK remains unknown. Ceramic additives in PEEK and PEKK have yielded mixed results, with some studies reporting an increase in strength [34, 35], while others report a decrease [36, 37]. It is hypothesized that the effect of the ceramic is contingent on whether the ceramic–polymer matrix effectively transfers stress from the polymer to the stronger ceramic, or if the interaction between the polymer and ceramic is limited [38]. Thus, establishing the impact of FFF printing parameters on the mechanical properties and crystallinity of Si_3N_4-PEKK is crucial to determining whether it can be printed with sufficient strength for medical implants.

We investigated FFF printing parameters for vertically oriented PEKK and Si_3N_4-PEKK using the Taguchi method to determine their mechanical strength, while also considering changes in thermal properties. The objectives of this study were: (1) Find the optimized FFF parameters for PEKK and Si_3N_4-PEKK. (2) Compare the mechanical properties of FFF printed PEKK and Si_3N_4-PEKK to neat injection-molded PEKK. (3) Determine the influence of printing parameters and the inclusion of silicon nitride on the thermal properties and crystallinity of PEKK.

2 | Materials and Methods

2.1 | Taguchi

The Taguchi method was selected to evaluate the impact of multiple printing parameters while minimizing the number of experiments. It is a statistical method that involves using an orthogonal array to efficiently test multiple parameters with a minimal number of conditional set-ups. Nozzle (340°C–400°C for PEKK and 380°C–420°C for Si_3N_4-PEKK), bed (130°C–170°C), chamber temperatures (110°C–150°C), and layer height (0.1–0.3 mm) were chosen for evaluation, as they were identified as key parameters in the relevant review literature [23–29, 31]. Each parameter was assessed at three levels across the printable range: low, medium, and high. An L9 orthogonal array was employed to evaluate four parameters across three levels (Table 1).

2.2 | Materials and Manufacture

For this study, a 60/40 terephthalic/isophthalic (T/I) implantable-grade PEKK filament (1.75 mm) was used (IMPEKK 3D-F-T, Seqens, Aramon, France). The Si_3N_4-PEKK filament (1.75 mm) was compounded using medical-grade PEKK pellets (IMPEKK, Seqens, Lyon, France) with silicon nitride powder (AP^2, Sintx Technologies, Salt Lake City, UT, USA) at 15 vol.% (~30 wt.%). Silicon nitride particles have a median (D50) particle size of 0.8 μm. Both filaments were dried prior to 3D printing at 100°C for 8–12 h to reduce potential impact from moisture. Pentagonal towers were printed in the Z-direction on a medical FFF printer (EXT 220 MED, 3D Systems, Munich, Germany) using predetermined printing parameters according to the Taguchi array (Figure 1A) while all other parameters remained constant. ISO 527 1BA [39] tensile specimens, with a nominal gauge length of 25 mm, were then machined via CNC from pentagonal towers (Figure 1B).

2.3 | Mechanical Testing

Specimens underwent tensile testing on a calibrated electromechanical MTS Exceed system (Exceed E43, MTS, Eden Prairie, MN, USA). Testing was performed according to ISO 517 at a

TABLE 1 | Taguchi parameters for PEKK and Si_3N_4-PEKK evaluated four printing parameters at three levels across nine conditions.

	Nozzle temperature (°C)				
Condition	**PEKK**	**Si_3N_4-PEKK**	**Bed temperature (°C)**	**Chamber temperature (°C)**	**Layer height (mm)**
1	340	380	130	110	0.1
2	340	380	150	130	0.2
3	340	380	170	150	0.3
4	370	400	130	130	0.3
5	370	400	150	150	0.1
6	370	400	170	110	0.2
7	400	420	130	150	0.2
8	400	420	150	110	0.3
9	400	420	170	130	0.1

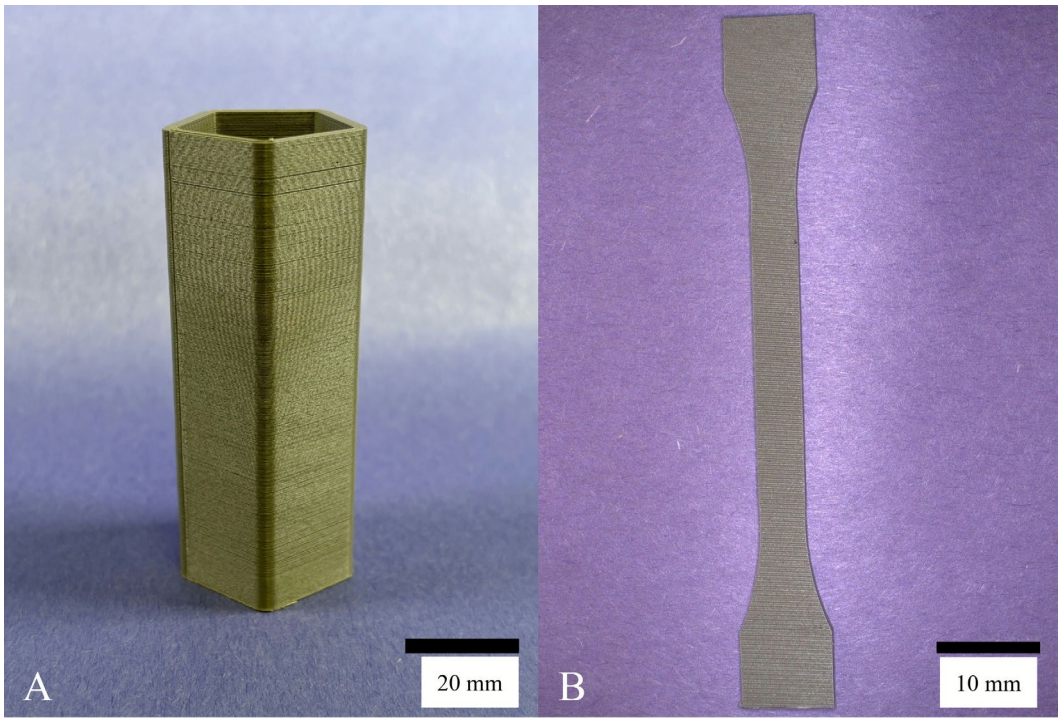

FIGURE 1 | Specimens were printed as pentagonal towers (A: Si_3N_4-PEKK tower) then machined into ISO 527 1BA [39] tensile specimens (B: Si_3N_4-PEKK tensile specimen).

test rate of 1 mm/min [39]. A calibrated extensometer (Model 3542, Epsilon, Jackson, WY, USA) was used for accurate strain measurements. Stress–strain curves were plotted from the data (Figures A1 and A2, Appendix A) and ultimate tensile strength (UTS), elastic modulus (E), yield strength, and strain at break values were calculated from the curves using a custom script in MATLAB 2023a (The MathWorks Inc., Natick, MA, USA), following the recommendations of ISO 527 as a guideline [39]. The modulus was determined as the slope of the first linear region and was used to calculate the 0.2% offset yield point (Appendix A). The ultimate tensile strength was identified at the peak stress of the stress–strain curves while the strain at break was identified as the final strain point (Table A1, Appendix A).

2.4 | DSC

Differential scanning calorimetry (DSC) was conducted on the highest strength (Condition 9, Table 1) and the lowest strength (Condition 3, Table 1) PEKK and Si_3N_4-PEKK printed samples ($n = 3$ each) in accordance with ASTM D3418 [40]. Technically Condition 3 was the second lowest strength for Si_3N_4-PEKK, but it was chosen to keep the conditions the same for both materials and will hereafter be referred to as the lowest strength condition. Three-millimeter round cylinders were punched from the grip region of the tensile specimens and after mass measurement, they underwent DSC analysis (TA Q2000 DSC with a RCS90 Cooler, TA Instruments, New Castle, DE, USA).

Samples were heated from 100°C to 400°C at a rate of 20°C/min. DSC analysis of the first heating trace was used to obtain the cold crystallization temperature (T_{cc}), melting temperature (T_m), and enthalpy (ΔH), where ΔH is the difference between the melting enthalpy (ΔH_m) and cold crystallization enthalpy (ΔH_{cc}). Crystallinity (X_c) was calculated using the following equation, where w is the weight fraction of the polymer and $\Delta H_{100\%}$ is the melting enthalpy of a theoretical 100% crystalline polymer. The $\Delta H_{100\%}$ for PEKK was 130 J/g [31, 32, 41].

$$X_c = \frac{\Delta H}{w\, x\, \Delta H_{100\%}} \times 100 \quad (1)$$

2.5 | Imaging

Digital optical microscopy (Keyence VHX-7000 digital optical microscope (DOM), Keyence Corp., Itasca, IL, USA) was used to image the fracture surfaces of the PEKK and Si_3N_4-PEKK tensile specimens following mechanical testing to examine failure mechanisms and imperfections, such as voids, resulting from the printing process. Additionally, specimens exhibiting notable features under DOM were further examined using scanning electron microscopy (Apreo 2S Lo Vac Scanning Electron Microscope (SEM) Thermo Fisher Scientific, Waltham, MA, USA) at higher magnification.

2.6 | Data Analysis

Using the Taguchi array set-up, signal/noise (S/N) ratios for UTS were calculated for each condition ($n = 9$, Table 1) using Equation (2), where C is the condition number, i is the sample number, n is the number of samples per condition, and Y_i is the UTS for each sample.

$$\frac{S}{N}_C = -10 \log \left[\frac{1}{n} \sum_{i=1}^{n} \frac{1}{Y_i^2} \right] \quad (2)$$

The S/N ratios were then averaged for each level ($n = 3$) of each print parameter ($n = 4$). The influence of each parameter was determined by calculating the delta (D), defined as the difference between the highest and lowest S/N ratios for that parameter.

$$D = \text{high}\frac{S}{N} - \text{low}\frac{S}{N} \quad (3)$$

Higher deltas show more impact on the UTS; therefore, the parameters were then assigned rankings (R) from one to four for the highest delta to the lowest. The mean (M) value of each condition was calculated using Equation (4), where i is the sample number, n is the number of samples per condition, and Y_i is the UTS for each sample. These means were then averaged across each level of each parameter.

$$M = \frac{1}{n} \sum_{i=1}^{n} \frac{1}{Y_i^2} \quad (4)$$

Normality was assessed using the Shapiro–Wilk test. UTS and E for both materials were compared via analysis of variance (ANOVA), followed by a post hoc Tukey Honest Significant Difference test. Taguchi parameter levels were compared via multifactorial ANOVA (Minitab 22.1, Minitab LLC, State College, PA, USA), using an alpha level of 0.05. Crystallinities of the highest and lowest strength PEKK and Si_3N_4-PEKK were compared via t-test (SPSS Statistics 29, IBM Corporation, Armonk, NY, USA).

3 | Results

3.1 | Taguchi and Mechanical Testing

UTS varied between 66.5 and 91.0 MPa for PEKK and 35.1 and 76.0 MPa for Si_3N_4-PEKK ($p < 0.001$ for both) showing the relevant impact of the processing parameters (Figure 2). The condition at which the highest performance was achieved for both materials (Condition 9: highest nozzle and bed temperatures, medium chamber temperature, and lowest layer height) was significantly stronger than all other conditions except Condition 5, which was the condition with the same layer height and lower nozzle and bed temperatures with higher chamber temperature (mean differences = 13.1, 12.4, 24.5, 24.0, 16.8, 10.1, and 23.4 MPa for PEKK and mean differences = 13.8, 18.6, 32.9, 30.6, 21.2, 20.6, and 41.0 MPa for Si_3N_4-PEKK Conditions 1–4 and 6–8, respectively, $p < 0.05$). Highest UTS (Condition 9 for both) for PEKK (91 MPa) reached 101% of the 90 MPa tensile strength value for the datasheet value of injection-molded PEKK [42], while Si_3N_4-PEKK (76.0 MPa) achieved 84% of the datasheet value. E varied between 2.7 and 3.0 GPa for PEKK and 3.0 and 4.3 GPa for Si_3N_4-PEKK ($p < 0.001$ for both) conditions. The stiffest condition for PEKK (Condition 7: highest nozzle and chamber temperatures, lowest bed temperature and medium layer height) was only significantly stiffer than Condition 3 (lowest nozzle temperature, highest chamber and bed temperatures), Condition 4 (medium nozzle temperature, lowest bed temperature, and medium chamber temperature), and Condition 8 (highest nozzle temperature, medium bed temperature, and lowest chamber temperature), which were the three conditions with the 0.3 mm layer height (0.3, 0.4, and 0.4 MPa, respectively, $p < 0.05$). The stiffest condition (Condition 9: highest nozzle and bed temperatures, medium chamber temperature, and lowest layer height) for Si_3N_4-PEKK was significantly stiffer than all 0.3 mm layer height conditions (Conditions 3, 4, 8, mean difference = 1.0, 1.0, and 1.3, $p < 0.05$) and two of three 0.2 mm layer height conditions (Conditions 2 and 6, mean difference = 0.4 and 0.5, respectively $p < 0.05$). Highest E for PEKK (3.0 GPa) reached 97% of the injection-molded PEKK, while highest Si_3N_4-PEKK (3.4 GPa) exceeded the datasheet value, reaching 139% [42].

Using the Taguchi array, S/N ratios were calculated and analyzed for UTS and E indicating that layer height had the greatest impact on the UTS and E, with a delta of 2.0 and 4.8 for PEKK and Si_3N_4-PEKK UTS, and delta values of 0.9 and 2.5 for PEKK and Si_3N_4-PEKK E, respectively (Table 2, Figure 3). A smaller layer height (0.1 mm) resulted in higher strength in both materials and higher modulus in Si_3N_4-PEKK than higher layer heights (0.2 and 0.3 mm), but it is important to note that reducing layer height increases print time. For example, printing the pentagonal towers with the lowest layer height (0.1 mm) took 3 h 23 min, whereas the highest layer height (0.3 mm) required 1 h 9 min. The second most influential parameter was chamber

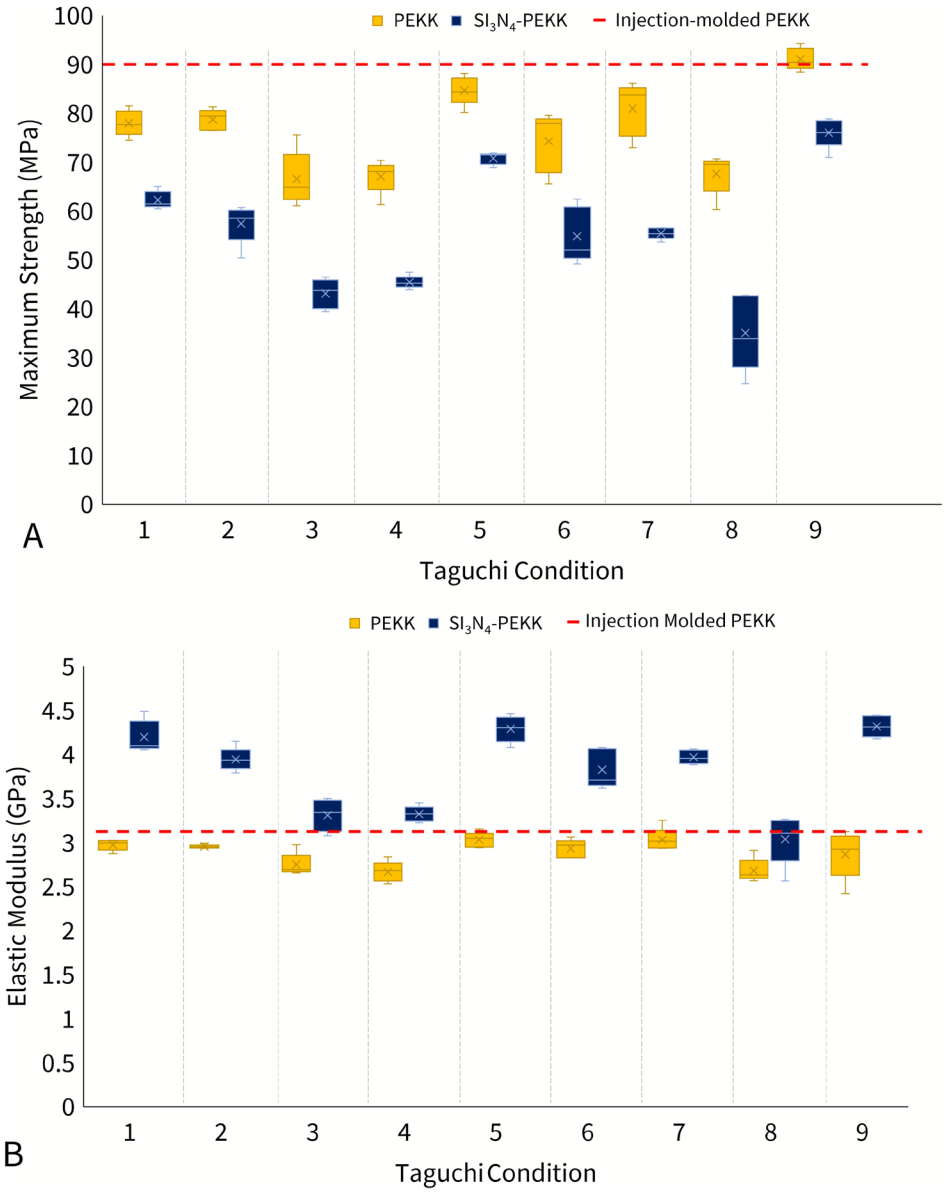

FIGURE 2 | Conventional box plots showed the range of ultimate tensile strength (UTS) (A) and elastic modulus (B) for conditions of PEKK and Si_3N_4-PEKK. UTS varied between 67 and 91 MPa for PEKK conditions and 35 and 76 MPa for Si_3N_4-PEKK conditions. Elastic modulus varied between 2.7 and 3.0 GPa for PEKK conditions and 3.0 and 4.3 GPa for Si_3N_4-PEKK conditions. The dashed line represents the UTS (A) and elastic modulus (B) of injection-molded neat PEKK [42].

temperature, with delta values of 0.6 and 1.7 for PEKK and Si_3N_4-PEKK UTS, and 0.4 and 0.5 for PEKK and Si_3N_4-PEKK E, respectively (Table 2). After layer height and chamber temperature, the third most influential parameter for PEKK UTS was nozzle temperature (delta = 0.6), followed by bed temperature (delta = 0.2). In contrast, for PEKK E and Si_3N_4-PEKK UTS and E, bed temperature was the third most influential (deltas = 0.15, 0.82, 0.25, respectively), with nozzle temperature being the least influential (deltas = 0.14, 0.67, and 0.17, respectively). For UTS, layer height, chamber temperature, and nozzle temperature were significant parameters for PEKK ($p < 0.001$, $p = 0.002$, and $p = 0.002$, respectively, Figure 3A), while layer height, chamber temperature, and bed temperature were significant parameters for Si_3N_4-PEKK ($p < 0.001$, $p < 0.001$, and $p = 0.020$, respectively, Figure 3B). UTS was strongest at layer heights of 0.1 mm and chamber temperatures of 130°C for both PEKK and Si_3N_4-PEKK (Table 2). The UTS was strongest for a nozzle temperature of 400°C for PEKK and a bed temperature of 170°C for Si_3N_4-PEKK. Only layer height was significantly impactful on E of PEKK ($p < 0.001$, Figure 3C), while both layer height and chamber temperature were significant parameters on E of Si_3N_4-PEKK ($p < 0.001$ and $p = 0.012$, respectively, Figure 3D). E was highest at layer heights of 0.2 mm for PEKK and 0.1 mm and chamber temperatures of 130°C for Si_3N_4-PEKK.

3.2 | DSC

Cold crystallization peaks (T_{cc}) were noted to occur in the first heating trace at significantly higher values for PEKK than for Si_3N_4-PEKK ($p < 0.001$ for both, mean = 263°C and 253°C, respectively.) (Figure 4, Table 3). Similarly, the melting

TABLE 2 | Signal/noise (S/N) ratios, deltas (*D*), and means (*M*) values for parameter levels for PEKK and Si_3N_4-PEKK ultimate tensile strength (UTS) and elastic modulus (*E*).

	PEKK				Si_3N_4-PEKK			
Parameter	**Level 1**	**Level 2**	**Level 3**	**Delta**	**Level 1**	**Level 2**	**Level 3**	**Delta**
UTS								
Nozzle temperature								
S/N ratios	37.38	37.46	37.95	0.57	34.54	34.93	34.27	0.67
Means	74.40	75.33	79.86		54.25	57.00	55.50	
Bed temperature								
S/N ratios	37.48	37.67	37.64	0.19	34.63	34.15	34.97	0.82
Means	75.32	76.98	77.28		54.36	54.41	57.98	
Chamber temperature								
S/N ratios	37.24	37.86	37.68	0.62	33.63	35.28	34.83	1.66
Means	73.27	78.94	77.37		50.71	59.61	56.44	
Layer height								
S/N ratios	38.51	37.79	36.48	2.03	36.82	34.89	32.04	4.78
Means	84.54	77.96	67.08		69.67	55.89	41.19	
E								
Nozzle temperature								
S/N ratios	9.21	9.15	9.06	0.14	11.57	11.56	11.40	0.17
Means	2.89	2.88	2.86		3.82	3.81	3.78	
Bed temperature								
S/N ratios	9.19	9.19	9.04	0.15	11.61	11.36	11.56	0.25
Means	2.89	2.89	2.85		3.83	3.76	3.82	
Chamber temperature								
S/N ratios	9.11	9.98	9.33	0.35	11.20	11.68	11.66	0.47
Means	2.86	2.83	2.94		3.69	3.86	3.86	
Layer height								
S/N ratios	9.37	9.45	8.60	0.85	12.59	11.83	10.11	2.48
Means	2.96	2.97	2.70		4.27	3.91	3.22	

temperature (T_m) for PEKK was significantly higher than that for Si_3N_4-PEKK ($p < 0.001$ for both, mean = 303°C and 313°C). It was found that Si_3N_4-PEKK differed significantly in percent crystallinity ($p < 0.001$, mean = 3.60%) when compared with PEKK (mean = 1.11%). However, the difference in crystallinity between the highest and lowest strength groups was not significant for both PEKK (mean = 1.18% and 1.04%, respectively) and Si3N4-PEKK (mean = 3.90% and 3.28%, respectively).

3.3 | Imaging

It was observed that the general mode of failure for both PEKK and Si_3N_4-PEKK was brittle fractures, with PEKK showing better layer-to-layer adhesion with breakages occurring both along and across the printed layers. Only a few of the strongest PEKK specimens (0.1 mm layer height) showed slight necking, in the fracture zone. The 0.1 mm layer height PEKK specimen showed greater adhesion across print lines with a smaller gap between print lines as seen in the 0.2 and 0.3 mm (Figure 5A–C) layer height specimens. In the Si_3N_4-PEKK specimens, the 0.2 and 0.3 mm layer height specimens (Figure 5E,F) showed voids that were not observed in the 0.1 mm layer height specimens (Figure 5D). When examined under SEM, it was observed that these voids were smooth in the 0.3 mm layer height specimen, indicating that they were likely air bubbles trapped during the printing process and not from silicon nitride particle pullout or from material transferring from one layer to another during fracture (Figure 5G). Additionally, the surface of the 0.1 mm layer height specimen showed a more uniform uneven surface from the material transfer of the Si_3N_4-PEKK layers pulling away from each other (Figure 5H).

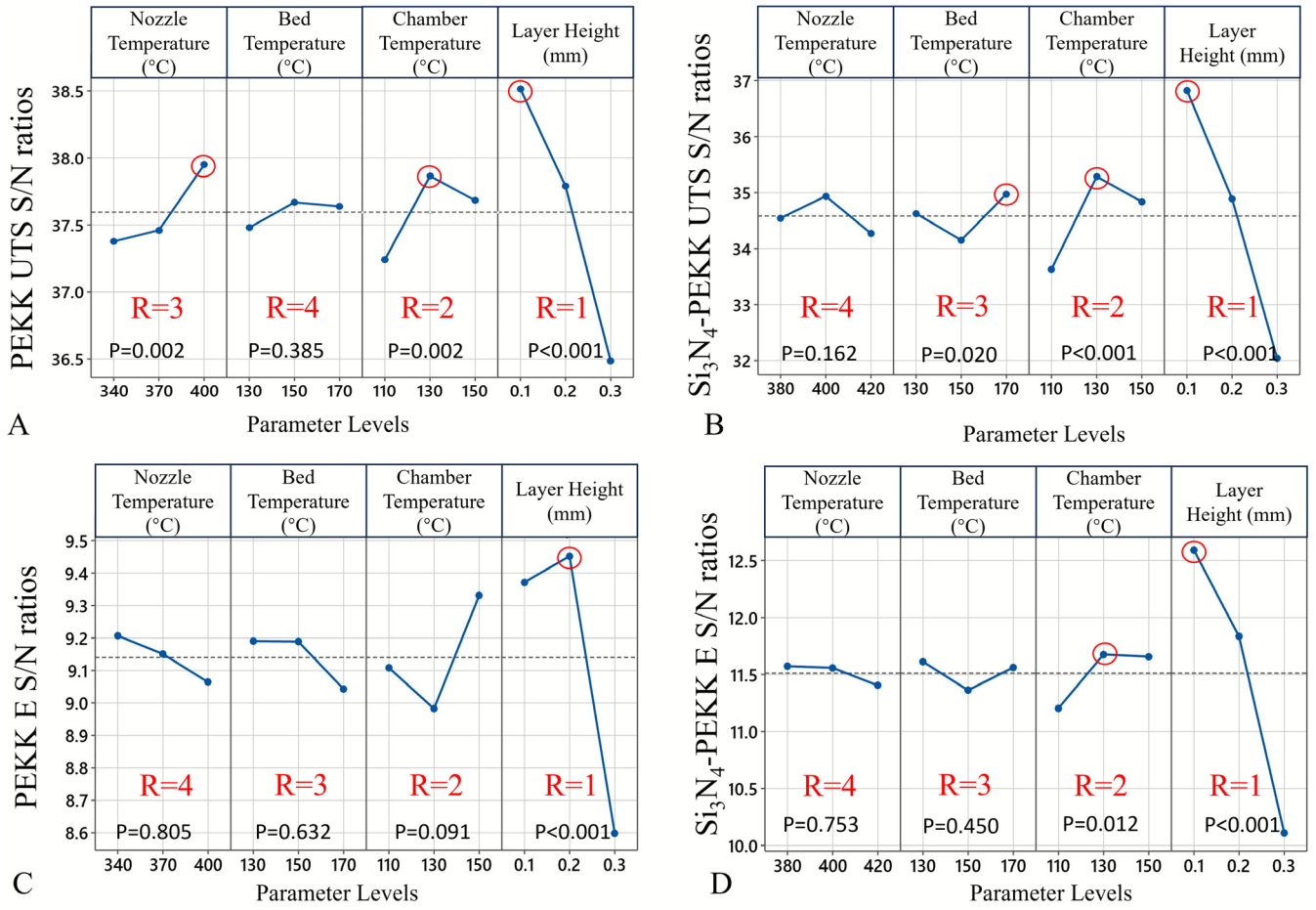

FIGURE 3 | Signal/noise (S/N) ratio plots for ultimate tensile strength (UTS) and for elastic modulus (E) showed that for PEKK (A and C) and Si_3N_4-PEKK (B and D) layer height was the most influential parameter as it had the highest ranking ($R=1$), followed by chamber temperature. Bed temperature and nozzle temperature were the third and fourth ranked influential parameters for both materials' E and Si_3N_4-PEKK UTS, while PEKK UTS showed the opposite. PEKK (A) exhibited the highest strength in layer heights of 0.1 mm, chamber temperatures of 130°C, and nozzle temperatures of 400°. Si_3N_4-PEKK (B) showed that the highest strength was obtained in layer heights of 0.1 mm, chamber temperatures of 130°C, and bed temperatures of 170°C. PEKK (C) displayed the highest modulus at layer heights of 0.2 mm, while Si_3N_4-PEKK (D) showed the highest modulus in layer heights of 0.1 mm and chamber temperatures of 130°C.

4 | Discussion

In this study, we analyzed the association of various printing parameters with the FFF of PEKK and Si_3N_4-PEKK specimens printed in the vertical direction to determine their mechanical feasibility for medical applications. PEKK specimens printed with statistically significant parameters achieved the datasheet value for tensile strength of injection-molded PEKK. The addition of Si_3N_4-PEKK reduced the strength of the specimens to 84% of the datasheet value. Highest strength was achieved across the selected parameters for both PEKK and Si_3N_4-PEKK with a layer height of 0.1 mm, a chamber temperature of 130°C, and a nozzle temperature of 400°C. The optimal bed temperature was 150°C for PEKK and 170°C for Si_3N_4-PEKK. The most influential printing parameter for both materials was the layer height which enforced fewer voids and gaps between print lines for both materials, followed by chamber temperature, then nozzle temperature in PEKK and bed temperature in Si_3N_4-PEKK. Crystallinity was not significantly affected by layer height, nozzle temperature, and chamber temperature for each material; however, the addition of Si_3N_4 resulted in a slight increase compared to PEKK.

There were several limitations to this study. First, this study focused solely on tensile testing, as it evaluates the weakest orientation, layer-to-layer adhesion that is critical for implant performance. However, future studies are needed to investigate the effects of printing parameters on PEKK and Si_3N_4-PEKK under compression, shear, and torsion, depending on the specific implant and its loading conditions in the body. Another limitation of this study is the need to have the Si_3N_4-PEKK filament manufactured by an external extrusion specialist, which resulted in some variability in filament consistency compared to the PEKK filament. To mitigate this, we conducted regular measurements of the filament diameter throughout the spool, ensuring that sections with diameter discrepancies outside the acceptable range were removed to maintain consistency during printing. The infeasibility of testing all the potential parameter combinations due to the large number of variables in 3D printing, each of which affects print quality and mechanical properties, is a further limitation. To address this, we focused on the most important and influential parameters identified in the literature [28, 29, 31]. To maintain a broad selection of parameters while keeping the number of tests manageable, we employed the Taguchi method for optimization. Additionally, control of

temperature, especially chamber temperature, is extremely important for crystallization and interlayer adhesion, which means that other parameters that increase time in the heated chamber could have a confounding effect on optimizing temperatures. However, we observed low crystallization after printing, even for longer prints, indicating that our chamber temperatures were too low for increased time in the print chamber to increase crystallinity. This indicated that parts can be removed from the printer directly following manufacture without having to spend additional time crystallizing, which decreases the manufacturing time of printed parts. Finally, while DSC is thought to estimate crystallinity at a higher value compared to other methods in PEEK, a similar polymer to PEKK, due to recrystallization during the heating process in the DSC scan [43], this method remains widely accepted for measuring crystallinity [29, 31, 32]. Furthermore, since all samples were analyzed using the same method, any overestimation is likely consistent across specimens, allowing for a valid comparison of the two materials and with other studies. It is also important to note that further work could be done to increase the crystallinity of both PEKK and Si_3N_4-PEKK by annealing the specimens, as found by Quiroga-Cortés and El Magri [31, 41].

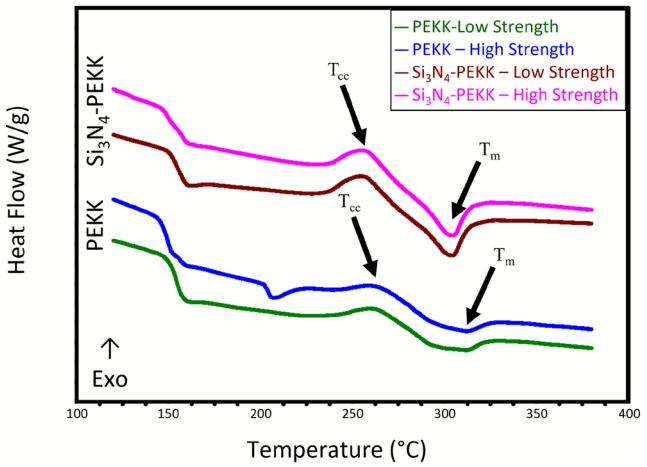

FIGURE 4 | Representative first heating trace from DSC for PEKK and Si_3N_4-PEKK with the highest strength (Condition 9: nozzle temperature 400°C/420°C, bed temperature 170°C, chamber temperature 130°C, layer height 0.1 mm) and lowest strength (Condition 3: nozzle temperature 340/380°C, bed temperature 170°C, chamber temperature 150°C, layer height 0.3 mm). Heat traces were vertically shifted for better visual representation. The addition of silicon nitride lowered both the cold crystallization temperature and melting temperatures.

The printing parameters analyzed in this study had a significant effect on the tensile strength and elastic modulus in both PEKK and Si_3N_4-PEKK. Layer height, followed by chamber temperature, was the most influential parameter for mechanical variables for both materials. Printing parameters had less effect on E than they did on the UTS. The highest UTS (91 MPa) and E (2.9 GPa) were achieved with a layer height of 0.1, a chamber temperature of 130°C and a nozzle temperature of 400°C for PEKK, while for Si_3N_4-PEKK, the same layer height and chamber temperature with a bed temperature of 170°C resulted in the highest tensile strength of 76 MPa and an elastic modulus of 4.3 GPa. Si_3N_4-PEKK specimens with a ceramic weight percentage of around 30%, were significantly weaker while being stiffer than the neat PEKK specimens, though they did reach 84% of the datasheet value strength of injection molded PEKK. The increase in modulus is well described in literature as many PAEK–ceramic composite studies have noted that the addition of ceramic particles stiffens the polymer matrix [35, 36, 38]. Several studies found initial increases in mechanical strength of PAEK composites with the initial addition of a ceramic additive that then led to a decrease in strength above certain ceramic loading levels [35, 38]. Similar to our results, Petrovic et al. [38] looked at ceramic weight percentages of 0%, 5%, 10%, 20%, and 40% and found a significant decrease in tensile strength with 40% weight in PEEK composites with β-tricalcium phosphate whereas an increase in strength was observed at levels up to 20 wt.%. Additionally, Gan et al. [35] noticed a drop-off in tensile strength at ceramic concentrations above 30% for a Mica-PEKK composite; however, it was still stronger than native PEKK. On the other hand, Manzoor et al. [36] showed that a lower ceramic (hydroxyapatite (HA)) weight percentage of 10% reduced the tensile strength of PEEK, which they attributed to poor interfacial bonding between the materials. Therefore, the decrease in mechanical strength in Si_3N_4-PEKK, could be caused by reduced bonding of the materials with the loading level of the ceramic. Careful consideration is required when incorporating ceramics, as the goal is to enhance antibacterial and osseointegrative properties while maintaining mechanical integrity. There exists a critical balance, and it is essential

TABLE 3 | Mean values ± standard deviation for cold crystallization temperature (T_{cc}), melting temperature (T_m), enthalpy (ΔH), and percent crystallinity (X_c) obtained from DSC for the PEKK and Si_3N_4-PEKK specimens with the highest (Condition 9: nozzle temperature 400°C/420°C, bed temperature 170°C, chamber temperature 130°C, layer height 0.1 mm) and the lowest ultimate strength (Condition 3: nozzle temperature 340°C/380°C, bed temperature 170°C, chamber temperature 150°C, layer height 0.3 mm).

Conditions	T_{cc} (°C)	T_m (°C)	ΔH (J/g)	X_c (%)
Highest strength				
PEKK	263 ± 0	312 ± 1	1.54 ± 0.10	1.18 ± 0.08
Si_3N_4-PEKK	253 ± 2	303 ± 1	3.55 ± 0.43	3.90 ± 0.48
Lowest strength				
PEKK	262 ± 2	313 ± 3	1.35 ± 0.31	1.04 ± 0.24
Si_3N_4-PEKK	252 ± 3	302 ± 0	2.99 ± 0.17	3.28 ± 0.18

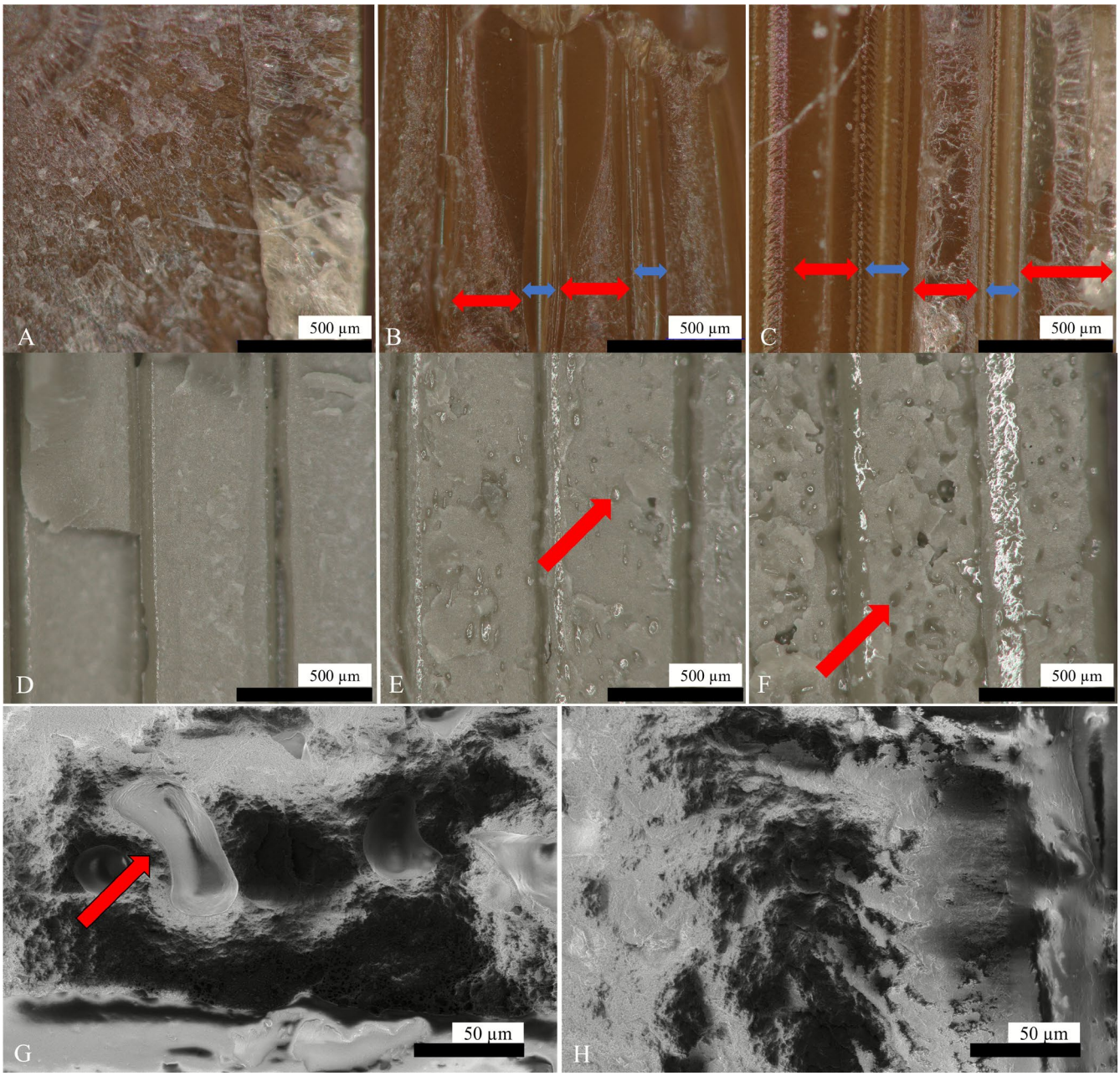

FIGURE 5 | PEKK fracture surfaces of print lines for parts with a layer height of 0.1 mm (A) showed no distinguishable print lines (red arrows) or gaps (blue arrows) between print lines, while 0.2 mm (B), and 0.3 mm (C) layer heights showed gaps that indicated less surface available for interlayer adhesion. Si_3N_4-PEKK fracture surfaces for parts with a layer height of 0.1 mm (D), 0.2 mm (E), and 0.3 mm (F) showed increased presence of features that appeared as voids (red arrows) with increased layer height. Scanning electron microscopy images showed smooth voids (arrow) were on the fracture surfaces of Si_3N_4-PEKK with layer heights of 0.3 mm (G), but no voids were observed for the specimens with layer heights of 0.1 mm (H).

to determine the extent to which mechanical strength can be compromised to achieve these benefits.

It was noted that the strongest parts and stiffest parts in both PEKK and Si_3N_4-PEKK had the lowest layer heights and the mid-range chamber temperature, with layer height having a greater effect. Similarly, Xu et al. [28] and Maloney et al. [29] observed a similar impact of layer height when testing the effect of FFF printing parameters on the flexural properties of PEKK, finding optimum layer heights of 0.1 mm. Additionally, Magri et al. [31] found an optimum layer height of 0.15 mm for flat printed PEKK tensile specimens. It is thought that this could be due to layer height affecting either the crystallinity of the part or the bonding area of the layers. On the other hand, little work has been done on the effect of chamber temperatures on 3D printed PAEKs. Yang et al. found that chamber temperatures while printing PEEK above its T_g increased crystallinity and tensile strength. However, with a 60/40 T/I ratio of PEKK, printing was not feasible due to material softening above the T_g. Additionally, since the crystallization kinetics of PEKK are different from PEEK, mechanical strength and interlayer bonding are not improved by the highest temperatures.

In this study low crystallinities, between 1.0% and 3.9%, were observed for high strength (Condition 9) and low strength (Condition 3) PEKK and Si_3N_4-PEKK specimens and both materials and conditions contained cold crystallization peaks around 260°C and 250°C, respectively. The presence of these cold crystallization peaks indicates that the printer conditions caused fast cooling rates that did not allow the time and energy for full chain rearrangement and crystallization, as similarly found in other PEKK printing studies, though the values were cooler between 210°C and 245°C [31, 32]. Similarly, Quiroga-Cortés et al. observed cold crystallization in cooling rates of 5°C or greater, with faster cooling rates and lower T/I ratios being associated with increased cold crystallization temperature. Additionally, it was noted that the cold crystallization peaks were not affected by high or low strength conditions but were affected by the inclusion of Si_3N_4-PEKK, with the Si_3N_4 reducing the temperature at which the peaks occurred. A similar 10°C shift was noted between PEKK and Si_3N_4-PEKK melting temperatures. The melt temperatures for the PEKK specimens were in the range that would be expected for PEKK with a 60/40 T/I ratio [32, 41]. The crystallinity also differed between materials, with PEKK only being slightly more than 1% crystalline, while Si_3N_4-PEKK with 15 vol.% (30 wt.%) silicon nitride had crystallinity between 3.3% and 3.9%. However, this increase in crystallinity in Si_3N_4-PEKK did not correlate to higher strength as it only reached 84% of the strength of neat PEKK. A study by Alamin et al. on zirconia-PEKK composites found that the addition of ceramic lowered the melting temperatures by between 2°C and 4°C, but they observed a decrease instead of an increase in crystallinity with increasing ceramic content. However, this study underwent a slow heating and cooling process significantly increasing the crystallinity of the neat PEKK when compared with our results, and consequently, their addition of ceramic impacted the ability of the matrix content to crystallize with the increasing grain size of the zirconia particles. In our case, without the right thermal conditions to encourage crystallinity in the neat PEKK, we saw increased crystallinity in the Si_3N_4-PEKK. This aligns with Javaid et al.'s observation of a decrease in melting temperature of a few degrees and an increase in crystallinity from 29.8% to 36.8% for 20% ceramic PEEK-Xonotlite. They additionally observed a decrease in strength from 127 MPa to 57 MPa for the composites. It was thought that this was due to the conflicting influence ceramic particles have on a polymer matrix as they create a nucleation site for crystals but also impede the mobility of the polymers and increase brittleness. While the ceramic addition of Si_3N_4 was associated with a slight increase in crystallinity, it was counteracted by an increase in brittleness of the specimens. For both materials, it was observed that the crystallinity for the stronger condition with a 0.1 mm layer height was slightly higher than the weaker condition with a 0.3 mm layer height but not significantly different. Xu et al. [28] suggested that lower layer heights created a compressive load on deposited filament affecting the crystallization of the parts, though they did not test for this. El Magri et al. [31] found a more noticeable increase in crystallinity from 6.8% to 8.7% with decreasing layer heights from 0.2 to 0.1 mm. However, they reported higher tensile strength of 84 MPa, compared with 70 and 79 MPa, in their flat printed parts with a 0.15 mm layer height, compared to 0.2 and 0.1 mm, which they suggested might have also been influenced by the interlayer adhesion of these parts. Therefore, it was concluded that while crystallinity might play a small role in the strength of the parts, interlayer adhesion was likely to play a larger role.

For PEKK, the lowest layer heights did not express the same level of voids and gaps between print lines as seen in those with greater layer heights. Xu et al. [28], in their study on the effect of printing parameters on PEKK, suggested that lower layer heights create a compressing load on deposited filament thereby creating a larger bonded surface area with fewer voids. Rashed et al. [32] also found that porosity and layer adhesion seemed to play a greater role in the tensile strength of FFF PEKK than crystallinity, which was not significantly higher in their stronger parts. In a follow-up study, they linked the most influential variable in compressive strength to porosity in the finished FFF PEKK parts [30]. Xu et al. and Maloney et al. [28, 29] observed similar behaviors of less porosity with lower layer heights. In this study, Si_3N_4-PEKK showed an interesting phenomenon where small features were noticed within the print lines for higher layer heights. These features in the Si_3N_4-PEKK were observed to have a smooth surface, indicating that they were caused by voids and not material transfer. Javaid et al. similarly found an irregular fracture surface in a PEEK-ceramic composite. In a recent study, Rashed et al. attempted to make a ceramic boron-carbide-PEKK filament and found 30–100 μm pores in the produced filament. They attributed the pores to entrapped pores during extrusion or created pores due to thermal gradients and residual stresses the material underwent while cooling. It is hypothesized that the FFF printing process for Si_3N_4-PEKK introduced micro voids, which may have been compacted or expelled when printed at lower printing heights.

In this study, printing parameters have been optimized for layer adhesion of PEKK and Si_3N_4-PEKK through tensile testing of vertically printed components. It is important in the future to examine the mechanical properties of the materials under other loading scenarios as might be experienced in 3D printed implants, such as compression, torsion, and shear. Additionally, as PEKK and Si_3N_4-PEKK have been shown to be largely amorphous via DSC results, annealing the parts post-printing could increase crystallinity and improve mechanical properties. Therefore, it would be advisable to explore the effect of annealing on both PEKK and Si_3N_4-PEKK.

5 | Conclusions

Layer height was the most influential printing parameter for both PEKK and Si_3N_4-PEKK UTS, followed by chamber temperature. Layer heights of 0.1 mm and chamber temperatures of 130°C resulted in improved strength for both materials. 3D-printed PEKK specimens, even when printed in the weakest orientation, were found to retain the strength of injection-molded PEKK parts if printed with the appropriate processing parameters [42]. With the addition of 15 vol.% Si_3N_4, the printed specimens still achieved 84% of the strength of injection-molded PEKK, demonstrating the potential of Si_3N_4-PEKK for load-bearing applications.

Funding

This research was funded by the National Institute of Dental and Craniofacial Research (NIDCR) under project 1R43DE031456-01.

Ethics Statement

The authors have nothing to report.

Consent

The authors have nothing to report.

Conflicts of Interest

Tabitha Derr reports a relationship with Sintx Technologies Inc. that includes employment. Cemile Basgul declares no known competing financial interests or personal relationships that could have appeared to influence the work reported in this paper. Paul DeSantis declares no known competing financial interests or personal relationships that could have appeared to influence the work reported in this paper. Ryan M. Bock reports a relationship with Sintx Technologies Inc. that includes employment and equity or stocks. Steven M. Kurtz reports a relationship with Gyroid LLC that includes: consulting or advisory, employment, and speaking and lecture fees. Steven M. Kurtz reports a relationship with Elsevier that includes: publishing royalties, financial and material support. Steven M. Kurtz reports general research support from: Celanese, Ceramtec, Invibio, Mitsubishi Chemical Advanced Materials, Orthofix, 3Spine, Seqens, DePuy Synthesis, Enovis, Orthoplastics, Sintx Technologies, Stryker, Wright Medical Technologies, and Zimmer Biomet.

Data Availability Statement

The data that support the findings of this study are available from the corresponding author upon reasonable request.

References

1. V. P. Mantripragada, B. Lecka-Czernik, N. A. Ebraheim, and A. C. Jayasuriya, "An Overview of Recent Advances in Designing Orthopedic and Craniofacial Implants," *Journal of Biomedical Materials Research. Part A* 101, no. 11 (2013): 3349–3364.

2. D. J. Hackett, A. C. Rothenberg, A. F. Chen, et al., "The Economic Significance of Orthopaedic Infections," *Journal of the American Academy of Orthopaedic Surgeons* 23, no. suppl (2015): S1–S7.

3. E. C. Rodríguez-Merchán, D. J. Davidson, and A. D. Liddle, "Recent Strategies to Combat Infections From Biofilm-Forming Bacteria on Orthopaedic Implants," *International Journal of Molecular Sciences* 22 (2021): 10243, https://doi.org/10.3390/ijms221910243.

4. M. Ishikawa, K. L. de Mesy Bentley, B. J. McEntire, B. S. Bal, E. M. Schwarz, and C. Xie, "Surface Topography of Silicon Nitride Affects Antimicrobial and Osseointegrative Properties of Tibial Implants in a Murine Model," *Journal of Biomedical Materials Research. Part A* 105, no. 12 (2017): 3413–3421.

5. G. Pezzotti, R. M. Bock, B. J. McEntire, et al., "Silicon Nitride Bioceramics Induce Chemically Driven Lysis in *Porphyromonas gingivalis*," *Langmuir* 32, no. 12 (2016): 3024–3035.

6. G. Pezzotti, "A Spontaneous Solid-State NO Donor to Fight Antibiotic Resistant Bacteria," *Materials Today Chemistry* 9 (2018): 80–90.

7. G. Pezzotti, "Silicon Nitride: A Bioceramic With a Gift," *ACS Applied Materials & Interfaces* 11, no. 30 (2019): 26619–26636.

8. R. M. Bock, E. N. Jones, D. A. Ray, B. Sonny Bal, G. Pezzotti, and B. J. McEntire, "Bacteriostatic Behavior of Surface Modulated Silicon Nitride in Comparison to Polyetheretherketone and Titanium," *Journal of Biomedical Materials Research Part A* 105, no. 5 (2017): 1521–1534.

9. F. Boschetto, "Surface Functionalization of PEEK With Silicon Nitride," *Biomedical Materials* 16, no. 1 (2020): 015015.

10. H. Wu, L. Yang, J. Qian, et al., "Microporous Coatings of PEKK/SN Composites Integration With PEKK Exhibiting Antibacterial and Osteogenic Activity, and Promotion of Osseointegration for Bone Substitutes," *ACS Biomaterials Science & Engineering* 5, no. 3 (2019): 1290–1301.

11. R. M. Bock, B. J. McEntire, B. S. Bal, M. N. Rahaman, M. Boffelli, and G. Pezzotti, "Surface Modulation of Silicon Nitride Ceramics for Orthopaedic Applications," *Acta Biomaterialia* 26 (2015): 318–330.

12. Z. Krstic and V. D. Krstic, "Silicon Nitride: The Engineering Material of the Future," *Journal of Materials Science* 47, no. 2 (2012): 535–552.

13. R. F. Heary, N. Parvathreddy, S. Sampath, and N. Agarwal, "Elastic Modulus in the Selection of Interbody Implants," *Journal of Spine Surgery* 3, no. 2 (2017): 163–167.

14. H. Spece, P. M. DeSantis, and S. M. Kurtz, "Development of an Architecture-Property Model for Triply Periodic Minimal Surface Structures and Validation Using Material Extrusion Additive Manufacturing With Polyetheretherketone (PEEK)," *Journal of the Mechanical Behavior of Biomedical Materials* 133 (2022): 105345.

15. N. Sharma, S. Aghlmandi, S. Cao, C. Kunz, P. Honigmann, and F. M. Thieringer, "Quality Characteristics and Clinical Relevance of In-House 3D-Printed Customized Polyetheretherketone (PEEK) Implants for Craniofacial Reconstruction," *Journal of Clinical Medicine* 9, no. 9 (2020): 2818.

16. N. Sharma, S. Aghlmandi, F. Dalcanale, et al., "Quantitative Assessment of Point-Of-Care 3D-Printed Patient-Specific Polyetheretherketone (PEEK) Cranial Implants," *International Journal of Molecular Sciences* 22, no. 16 (2021): 8521.

17. C. Basgul, T. Yu, D. W. MacDonald, R. Siskey, M. Marcolongo, and S. M. Kurtz, "Structure–Property Relationships for 3D-Printed PEEK Intervertebral Lumbar Cages Produced Using Fused Filament Fabrication," *Journal of Materials Research* 33, no. 14 (2018): 2040–2051.

18. C. Basgul, D. W. MacDonald, R. Siskey, and S. M. Kurtz, "Thermal Localization Improves the Interlayer Adhesion and Structural Integrity of 3D Printed PEEK Lumbar Spinal Cages," *Materialia* 10 (2020): 100650.

19. X. Zhao, D. Xiong, and Y. Liu, "Improving Surface Wettability and Lubrication of Polyetheretherketone (PEEK) by Combining With Polyvinyl Alcohol (PVA) Hydrogel," *Journal of the Mechanical Behavior of Biomedical Materials* 82 (2018): 27–34.

20. A. Maloney, I. Major, N. Gately, and D. M. Devine, "Exploring Process–Structure–Property Relationships of PEKK and PEEK in Fused Filament Fabrication," *Journal of Applied Polymer Science* 142, no. 34 (2025): e57347.

21. M. Wang, G. Bhardwaj, and T. J. Webster, "Antibacterial Properties of PEKK for Orthopedic Applications," *International Journal of Nanomedicine* 12 (2017): 6471–6476.

22. B. Yuan, Q. Cheng, R. Zhao, et al., "Comparison of Osteointegration Property Between PEKK and PEEK: Effects of Surface Structure and Chemistry," *Biomaterials* 170 (2018): 116–126.

23. C. Yang, X. Tian, D. Li, Y. Cao, F. Zhao, and C. Shi, "Influence of Thermal Processing Conditions in 3D Printing on the Crystallinity and Mechanical Properties of PEEK Material," *Journal of Materials Processing Technology* 248 (2017): 1–7.

24. P. Wang, B. Zou, H. Xiao, S. Ding, and C. Huang, "Effects of Printing Parameters of Fused Deposition Modeling on Mechanical Properties, Surface Quality, and Microstructure of PEEK," *Journal of Materials Processing Technology* 271 (2019): 62–74.

25. A. El Magri, K. El Mabrouk, S. Vaudreuil, H. Chibane, and M. E. Touhami, "Optimization of Printing Parameters for Improvement of Mechanical and Thermal Performances of 3D Printed Poly(Ether Ether Ketone) Parts," *Journal of Applied Polymer Science* 137, no. 37 (2020): 49087.

26. C.-P. Jiang, Y. C. Cheng, H. W. Lin, Y. L. Chang, T. Pasang, and S. Y. Lee, "Optimization of FDM 3D Printing Parameters for High Strength PEEK Using the Taguchi Method and Experimental Validation," *Rapid Prototyping Journal* 28, no. 7 (2022): 1260–1271.

27. A. Pulipaka, K. M. Gide, A. Beheshti, and Z. S. Bagheri, "Effect of 3D Printing Process Parameters on Surface and Mechanical Properties of FFF-Printed PEEK," *Journal of Manufacturing Processes* 85 (2023): 368–386.

28. C. Xu, "Effect of Processing Parameters on Flexural Properties of 3D-Printed Polyetherketoneketone Using Fused Deposition Modeling," *Polymer Engineering and Science* 61, no. 2 (2020): 465–476.

29. A. Maloney, I. Major, N. Gately, and D. M. Devine, "Effects of 3D Printing Parameters on the Flexural Properties of Semi-Crystalline PEKK," *Materials Today Communications* 42 (2025): 111152.

30. K. Rashed, A. Kafi, R. Simons, and S. Bateman, "Optimization of Material Extrusion Additive Manufacturing Process Parameters for Polyether Ketone Ketone (PEKK)," *International Journal of Advanced Manufacturing Technology* 126, no. 3 (2023): 1067–1091.

31. A. El Magri, S. Vaudreuil, A. B. Ayad, A. El Hakimi, E. O. Rabie, and D. Amegouz, "Effect of Printing Parameters on Tensile, Thermal and Structural Properties of 3D-Printed Poly (Ether Ketoneketone) PEKK Material Using Fused Deposition Modeling," *Journal of Applied Polymer Science* 140 (2023): e54078.

32. K. Rashed, A. Kafi, R. Simons, and S. Bateman, "Effects of Fused Filament Fabrication Process Parameters on Tensile Properties of Polyether Ketone Ketone (PEKK)," *International Journal of Advanced Manufacturing Technology* 122, no. 9 (2022): 3607–3621.

33. L. Doyle, X. Pérez-Ferrero, J. García-Molleja, R. Losada, P. Romero-Rodríguez, and J. P. Fernández-Blázquez, "Fused Filament Fabrication of Slow-Crystallizing Polyaryletherketones: Crystallinity and Mechanical Properties Linked to Processing and Post-Treatment Parameters," *Polymers* 16, no. 23 (2024): 3354.

34. P. R. Monich, B. Henriques, A. P. Novaes de Oliveira, J. C. M. Souza, and M. C. Fredel, "Mechanical and Biological Behavior of Biomedical PEEK Matrix Composites: A Focused Review," *Materials Letters* 185 (2016): 593–597.

35. D. Gan, S. Lu, C. Song, and Z. Wang, "Morphologies, Mechanical Properties and Wear of Poly(Ether Ketone Ketone) (PEKK) and Its Composites Reinforced With Mica," *Macromolecular Materials and Engineering* 286, no. 5 (2001): 296–301.

36. F. Manzoor, A. Golbang, S. Jindal, et al., "3D Printed PEEK/HA Composites for Bone Tissue Engineering Applications: Effect of Material Formulation on Mechanical Performance and Bioactive Potential," *Journal of the Mechanical Behavior of Biomedical Materials* 121 (2021): 104601.

37. S. Javaid, M. Dey, C. Matzke, and S. Gupta, "Synthesis and Characterization of Engineered PEEK-Based Composites for Enhanced Tribological and Mechanical Performance," *Journal of Applied Polymer Science* 139, no. 39 (2022): e52886.

38. L. Petrovic, D. Pohle, H. Münstedt, T. Rechtenwald, K. A. Schlegel, and S. Rupprecht, "Effect of βTCP Filled Polyetheretherketone on Osteoblast Cell Proliferation In Vitro," *Journal of Biomedical Science* 13, no. 1 (2006): 41–46.

39. *527-1, I., Plastics - Determination of Tensile Properties* (International Organization of Standardization, 2019).

40. *D3418-21, A.S., Standard Test Method for Transition Temperatures and Enthalpies of Fusion and Crystallization of Polymers by Differential Scanning Calorimetry* (ASTM International, 2021).

41. L. Quiroga Cortés, N. Caussé, E. Dantras, A. Lonjon, and C. Lacabanne, "Morphology and Dynamical Mechanical Properties of Poly Ether Ketone Ketone (PEKK) With Meta Phenyl Links," *Journal of Applied Polymer Science* 133, no. 19 (2016): 43396.

42. SEQENS, Technical Data – IMPEKK® 3D-F (2022).

43. M. Doumeng, L. Makhlouf, F. Berthet, et al., "A Comparative Study of the Crystallinity of Polyetheretherketone by Using Density, DSC, XRD, and Raman Spectroscopy Techniques," *Polymer Testing* 93 (2021): 106878.

Appendix A

Additional Data From PEKK and Si_3N_4-PEKK Mechanical Testing

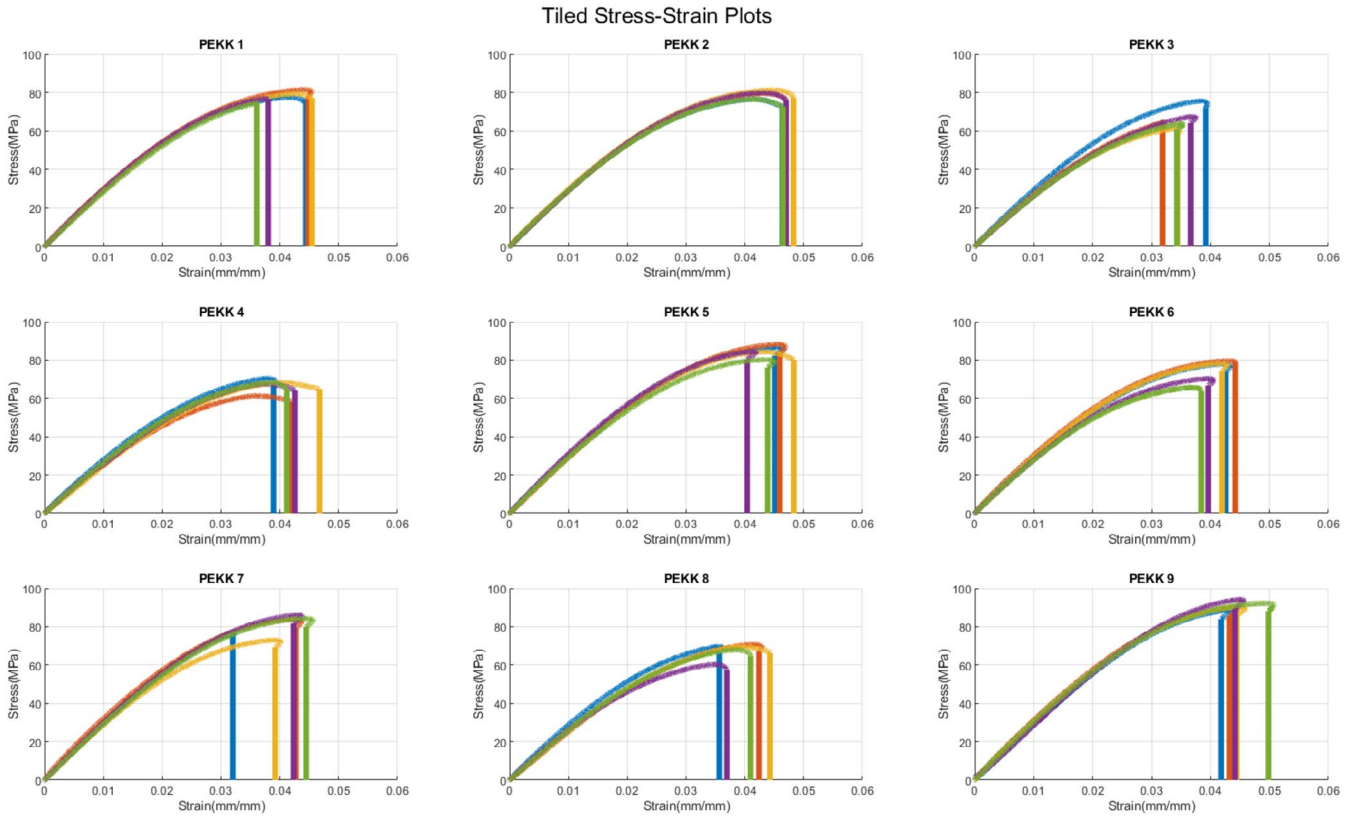

FIGURE A1 | Stress–strain curves for PEKK tensile specimens.

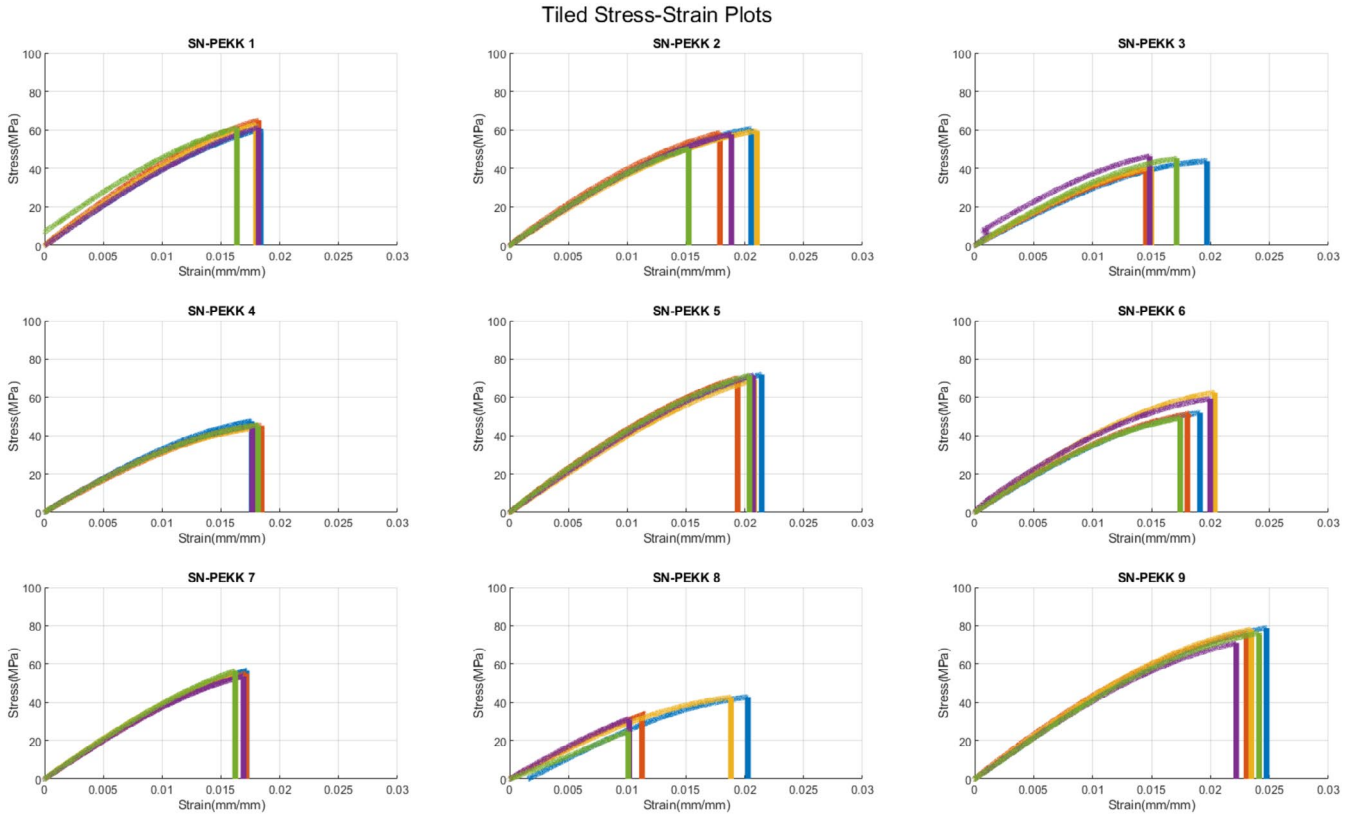

FIGURE A2 | Stress–strain curves for Si_3N_4-PEKK tensile specimens.

TABLE A1 | Ultimate tensile strength, yield strength, elastic modulus, and strain at break for PEKK and Si_3N_4-PEKK specimens. Yield strength followed a similar trend to UTS with Si_3N_4-PEKK values lower than PEKK and Condition 9 as the strongest for both materials. The Si_3N_4-PEKK material was observed as stiffer than PEKK with a lower strain at break for all conditions.

	Ultimate tensile strength (MPa)		Yield strength (MPa)		Elastic modulus (GPa)		Strain at break (mm/mm)	
Condition	**PEKK**	**Si_3N_4-PEKK**	**PEKK**	**Si_3N_4-PEKK**	**PEKK**	**Si_3N_4-PEKK**	**PEKK**	**Si_3N_4-PEKK**
1	77.9 ± 2.6	62.2 ± 1.8	53.0 ± 0.7	56.1 ± 1.1	3.0 ± 0.1	4.2 ± 0.2	0.042 ± 0.004	0.018 ± 0.001
2	78.7 ± 2.1	57.4 ± 4.1	53.2 ± 1.2	50.1 ± 1.4	3.0 ± 0.0	3.9 ± 0.1	0.047 ± 0.001	0.019 ± 0.002
3	66.5 ± 5.6	43.1 ± 3.0	46.6 ± 3.1	39.9 ± 1.9	2.7 ± 0.1	3.3 ± 0.2	0.035 ± 0.002	0.016 ± 0.002
4	67.1 ± 3.4	45.4 ± 1.3	46.4 ± 2.4	40.2 ± 1.3	2.7 ± 0.1	3.3 ± 0.1	0.042 ± 0.003	0.018 ± 0.000
5	84.6 ± 3.0	70.8 ± 1.2	57.2 ± 2.4	61.4 ± 1.2	3.0 ± 0.1	4.3 ± 0.1	0.045 ± 0.003	0.021 ± 0.001
6	74.3 ± 6.1	54.8 ± 5.7	50.0 ± 2.5	47.1 ± 3.4	2.9 ± 0.1	3.8 ± 0.2	0.041 ± 0.002	0.019 ± 0.001
7	80.9 ± 5.5	55.4 ± 1.2	55.9 ± 4.0	52.0 ± 1.7	3.0 ± 0.1	4.0 ± 0.1	0.040 ± 0.004	0.017 ± 0.000
8	67.6 ± 4.2	35.1 ± 7.7	47.6 ± 3.2	37.1 ± 0.1	2.9 ± 0.3	3.0 ± 0.3	0.040 ± 0.003	0.014 ± 0.004
9	91.0 ± 2.3	76.0 ± 3.1	66.5 ± 5.1	62.2 ± 1.8	2.9 ± 0.3	4.3 ± 0.1	0.045 ± 0.003	0.024 ± 0.001